

# Dalton Transactions

An international journal of inorganic chemistry

Accepted Manuscript

This article can be cited before page numbers have been issued, to do this please use: J. García, P. Escamilla, J. Ferrando-Soria, T. M. Grancha, D. Armentano and E. Pardo, *Dalton Trans.*, 2026, DOI: 10.1039/D6DT01043A.



This is an Accepted Manuscript, which has been through the Royal Society of Chemistry peer review process and has been accepted for publication.

Accepted Manuscripts are published online shortly after acceptance, before technical editing, formatting and proof reading. Using this free service, authors can make their results available to the community, in citable form, before we publish the edited article. We will replace this Accepted Manuscript with the edited and formatted Advance Article as soon as it is available.

You can find more information about Accepted Manuscripts in the [Information for Authors](#).

Please note that technical editing may introduce minor changes to the text and/or graphics, which may alter content. The journal's standard [Terms & Conditions](#) and the [Ethical guidelines](#) still apply. In no event shall the Royal Society of Chemistry be held responsible for any errors or omissions in this Accepted Manuscript or any consequences arising from the use of any information it contains.

## ARTICLE

## Multivariate Sulfur-Functionalized MOFs Shaped into Alginate Spheres for Robust and Reusable Multidye Water Remediation

Jaume García,<sup>†a</sup> Paula Escamilla,<sup>†b</sup> Jesús Ferrando-Soria,<sup>\*a</sup> Thais Grancha,<sup>a</sup> Donatella Armentano<sup>\*c</sup> and Emilio Pardo<sup>\*a</sup>

Received 00th January 20xx,  
Accepted 00th January 20xx

DOI: 10.1039/x0xx00000x

The removal of synthetic organic dyes from contaminated water remains a major environmental challenge, particularly under multicomponent and real-water conditions. Herein, we report a scalable adsorption platform based on sulfur-functionalized metal–organic frameworks (MOFs) for efficient multidye removal. Three isorecticular MOFs, including a multivariate analogue incorporating methylcysteine and methionine functionalities, were evaluated using real water (Turia River, Spain). The multivariate MOF shows faster adsorption kinetics and achieves quantitative dye removal, outperforming its monofunctional counterparts. For practical implementation, the MOFs were immobilized into calcium alginate spherical beads ( $\approx 50$  wt% loading), yielding mechanically robust composites that preserve crystallinity and porosity. The shaped materials retain high adsorption efficiency and can be reused over multiple cycles without performance loss. Under continuous-flow solid-phase extraction conditions, the system achieves  $>99\%$  removal for all dyes, enabling rapid and effective water decontamination.

### 1. Introduction

The contamination of water resources by synthetic organic dyes<sup>1</sup> represents a persistent environmental challenge due to their extensive use in textile, paper, pharmaceutical and bioimaging industries.<sup>2</sup> Even at very low concentrations, dyes impart intense coloration to water streams, reducing light penetration and adversely affecting aquatic ecosystems,<sup>3</sup> while many of them also present toxic or mutagenic effects.<sup>4</sup> The chemical stability and structural diversity of dyes further complicate their removal by conventional treatment methods.<sup>5</sup> In this context, the development of efficient, reusable and sustainable strategies for dye removal remains a priority for modern water remediation technologies.<sup>6</sup>

Among the different approaches explored for dye removal,<sup>5,6</sup> adsorption<sup>7,8</sup> stands out as an attractive and widely applicable strategy owing to its operational simplicity, high efficiency and compatibility with existing treatment infrastructures.<sup>9,10</sup> Importantly, adsorption-based processes can be implemented under mild conditions and do not generate harmful transformation byproducts.<sup>11</sup> However, the sustainability and practical relevance of adsorption technologies critically depend on the availability of adsorbent

materials that combine high uptake capacity, fast kinetics, long-term reusability and straightforward recovery from aqueous media.<sup>11</sup>

Metal–organic frameworks (MOFs)<sup>12–15</sup> have emerged as a versatile class of adsorbent materials for water remediation due to their exceptionally high surface areas, well-defined porosity and modular chemical tunability.<sup>16–19</sup> The possibility of incorporating specific functional groups into MOF structures has enabled the rational design of materials with enhanced affinity toward targeted pollutants,<sup>20,21</sup> including organic dyes<sup>22,23</sup> and other emerging contaminants.<sup>24</sup> Despite these advantages, most MOF-based adsorption studies are often conducted using microcrystalline powders,<sup>25</sup> which pose significant challenges in terms of handling, separation and scalability.<sup>25</sup> These limitations strongly hinder the translation of highly active MOFs from laboratory studies to practical water treatment systems.<sup>26</sup>

To address these challenges, considerable effort has been devoted to shaping<sup>27–29</sup> MOFs into macroscopic and mechanically robust forms, such as mixed-matrix membranes,<sup>30</sup> polymer foams<sup>31</sup> or pelletized composites.<sup>32</sup> These approaches represent important steps toward practical implementation, yet they often involve complex fabrication processes and may compromise the intrinsic properties of the MOF through pore blockage, reduced accessibility or slower adsorption kinetics.<sup>27</sup> Consequently, there remains a clear need for simple, low-cost and scalable processing strategies that enable MOFs to be deployed in macroscopic forms without sacrificing their adsorption performance or structural integrity.<sup>27–29</sup>

Calcium alginate<sup>33</sup> offers a particularly attractive platform for this purpose. As a naturally derived, inexpensive and environmentally benign biopolymer, alginate can be processed

<sup>a</sup> Instituto de Ciencia Molecular (ICMol), Universidad de Valencia, 46980 Paterna, Valencia, Spain. E-mail: [jesus.ferrando@uv.es](mailto:jesus.ferrando@uv.es); [emilio.pardo@uv.es](mailto:emilio.pardo@uv.es)

<sup>b</sup> Centro Singular de Investigación en Química Biolóxica e Materiais Moleculares (CIQUS), Universidade de Santiago de Compostela, 15782 Santiago de Compostela, Spain.

<sup>c</sup> Dipartimento di Chimica e Tecnologie Chimiche (CTC), Università della Calabria, Rende 87036, Cosenza, Italy. E-mail: [Donatella.armentano@unical.it](mailto:Donatella.armentano@unical.it)

<sup>†</sup> Electronic supplementary information (ESI) available. See DOI: 10.1039/x0xx00000x

<sup>\*</sup>These authors have equally contributed to this work



in aqueous media under mild conditions, aligning well with the principles of sustainable chemistry.<sup>34</sup> Upon crosslinking with divalent cations, alginate readily forms mechanically stable spherical beads<sup>35</sup> that can be easily handled, recovered and integrated into flow-through systems such as solid-phase extraction (SPE). These features make alginate-based spheres highly appealing for water remediation applications.<sup>36</sup> Nevertheless, demonstrating that highly active MOFs can be incorporated into alginate matrices while fully retaining their crystallinity, porosity and adsorption efficiency remains a critical challenge.<sup>36</sup>

In parallel with processing considerations, the molecular-level design of MOFs plays a crucial role in achieving high adsorption performance. Multivariate MOFs<sup>37,38</sup> (MTV-MOFs), which incorporate multiple functional groups within a single framework, have attracted growing attention due to their ability to create chemically diverse adsorption environments and promote synergistic interactions with target pollutants.<sup>39</sup> Such functional heterogeneity is particularly advantageous for the removal of complex contaminant mixtures, where different adsorption mechanisms may operate simultaneously. However, the integration of MTV-MOFs into processable and sustainable adsorbent platforms has so far been scarcely explored.<sup>40</sup>

Herein, we report a systematic study combining molecular design and sustainable processing to advance the practical use of MOFs in water remediation. For this purpose, three previously reported<sup>40–43</sup> sulfur-functionalized MOFs—including two monofunctional materials bearing methylcysteine or methionine residues and a multivariate MOF combining both functionalities within the same framework (Scheme S1 and Fig.

1)— have been selected. Their adsorption performance is evaluated toward a multidye complex water matrix, revealing a clear enhancement for the MTV-MOF that is attributed to functional synergy, in line with previous observations.<sup>39,44</sup> Crucially, these MOFs are processed into calcium alginate spheres that preserve the crystallinity, porosity and adsorption efficiency of the corresponding powdered materials. The resulting spherical adsorbents exhibit fast and quantitative dye removal,<sup>45,46</sup> excellent recyclability and structural robustness, highlighting alginate-based shaping as a sustainable and effective strategy to bridge advanced MOF design with realistic water remediation technologies.<sup>16</sup>

## 2. Results and discussion

In this work, we investigate the adsorption performance and processability of sulfur-functionalized metal–organic frameworks (MOFs) for water remediation applications. Thus, three previously reported oxamidato-based MOFs<sup>40,42</sup> derived from the amino acids *S*-methyl-*L*-cysteine and *L*-methionine—including two monofunctional materials bearing exclusively *S*-methyl-*L*-cysteine (**1**) or *L*-methionine (**2**) residues and also a multivariate MOF (**3**) combining 50% of both functionalities (–CH<sub>2</sub>SCH<sub>3</sub> and –CH<sub>2</sub>CH<sub>2</sub>SCH<sub>3</sub>) in a 1:1 ratio within the same framework (Fig. 1)— were employed. The three materials were selected to enable a systematic comparison between monofunctional and multivariate pore environments and to assess the impact of functional heterogeneity on dye adsorption performance.

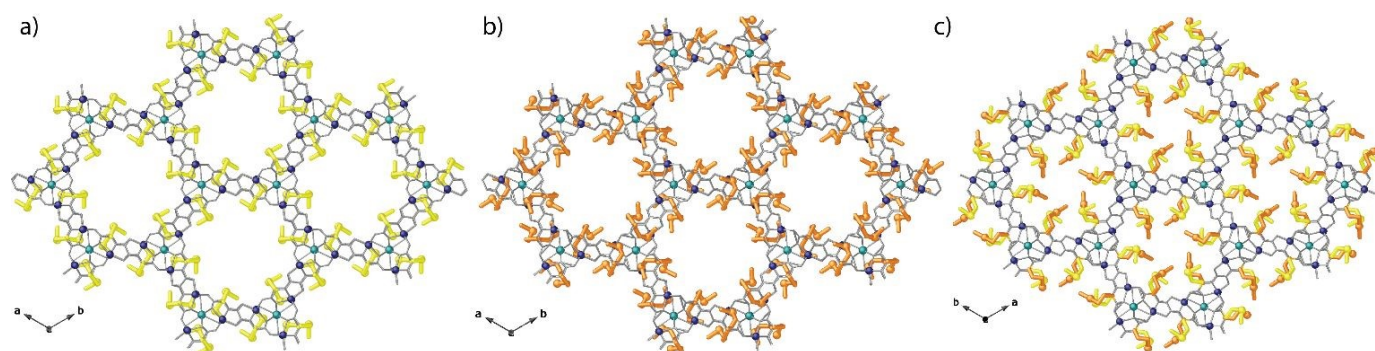


**Fig. 1.** Perspective views of the crystal structures of MOFs **1** (a), **2** (b) and MTV-MOF **3** (c). Metal atoms are represented as blue (Ca<sup>II</sup>) and cyan (Zn<sup>II</sup>) spheres whereas organic ligands are represented as thin grey sticks with the exception of amino acid residues, which are depicted as yellow (–CH<sub>2</sub>SCH<sub>3</sub> from *S*-Methyl-*L*-cysteine) and orange (–CH<sub>2</sub>CH<sub>2</sub>SCH<sub>3</sub> from *L*-methionine) thick sticks to emphasize the functionalization of the channels.

The study was conducted with three main objectives: (i) to evaluate the efficiency of the powdered crystalline MOFs toward the capture of organic dyes from aqueous media, with particular emphasis on the role of dual functionalization in the multivariate MOF **3**; (ii) to process these MOFs into calcium alginate spheres in order to obtain macroscopic, mechanically robust composites suitable for practical handling and implementation in capture devices; and (iii) to assess whether the adsorption properties observed for the powdered materials are fully retained upon shaping, thereby demonstrating the

effective translation of intrinsic MOF performance into processed and reusable adsorbents.

### 2.1 Synthesis and characterization

MOFs **1** and **2**, together with the multivariate analogue **3**, were prepared following the same previously established synthetic procedure that enables their isolation as gram-scale polycrystalline powders as well as single crystals suitable for structural analysis using slow diffusion methods (see Experimental Section). The materials correspond to the formulations {Ca<sup>II</sup>Zn<sup>II</sup><sub>6</sub>[(*S,S*)-Mecysmox]<sub>3</sub>(OH)<sub>2</sub>(H<sub>2</sub>O)} · 12H<sub>2</sub>O<sup>47</sup>



(1),  $\{Ca^{II}Zn^{II}_6[(S,S)\text{-methox}]_3(OH)_2(H_2O)\} \cdot 16H_2O$ <sup>42</sup> (2) and  $\{Ca^{II}Zn^{II}_6[(S,S)\text{-methox}]_{1.5}[(S,S)\text{-Mecysmox}]_{1.5}(OH)_2(H_2O)\} \cdot 12H_2O$ <sup>40</sup> (3), where Mecysmox and methox denote bis[(S)-methylcysteine]oxalyldiamide and bis[(S)-methionine]oxalyldiamide ligands, respectively.

Prior to evaluating their adsorption performance, the crystallinity, phase purity and permanent porosity of 1–3 were assessed using C, H, S, N analyses (see experimental section), powder X-ray diffraction (PXRD) and N<sub>2</sub> adsorption measurements on freshly prepared polycrystalline samples. The PXRD patterns (Figs. S1–S2, see ESI<sup>†</sup>) confirm the phase purity of all materials and their isorecticular relationship. Nitrogen adsorption isotherms recorded at 77 K closely match those previously reported for 1–3<sup>40,42</sup> (Fig. S3), indicating preservation of the porous frameworks. The Brunauer–Emmett–Teller (BET) surface areas<sup>48</sup> were determined to be 725, 451 and 664 m<sup>2</sup> g<sup>-1</sup> for MOFs 1–3, respectively.

Fig. 1 depicts the crystal structures of MOFs 1–3, which are all isomorphous and crystallize in the chiral P6<sub>3</sub> space group of the hexagonal system. The three materials are based on chiral three-dimensional bimetallic (Ca<sup>II</sup>-Zn<sup>II</sup>) networks featuring one-dimensional medium-sized hexagonal channels, whose internal surfaces are functionalized by the corresponding sulfur-containing amino acid residues.

In particular, the crystal structure of the multivariate framework 3 (Fig. 1c) clearly reveals medium-sized hexagonal channels simultaneously decorated by methionine and methylcysteine residues, unambiguously confirming the incorporation of both ligands within the same framework and

giving rise to a chemically heterogeneous pore environment. As in the parent monofunctional materials 1 and 2, the framework of 3 is structurally robust, with conformational flexibility largely confined to the pendant thioether side chains lining the pores. Based on previous studies on related sulfur-functionalized MOFs, such flexible thioether functionalities present in 1–3 are expected to engage in a range of noncovalent interactions with organic guests, including van der Waals contacts, hydrogen bonding, and  $\sigma$ -hole interactions. These interactions are anticipated to provide adaptable adsorption sites while preserving the structural integrity of the framework.<sup>49–52</sup>

## 2.2 Capture experiments of powdered samples.

At this stage, the capture efficiencies of polycrystalline powdered samples of 1–3 were evaluated using a multidye environmental aqueous solution (Turia river, Valencia, Spain, 39.5463° N, -0.5477° W) containing methylene blue (MB), brilliant green (BG), pyronine Y (PY) and auramine O (AO) (10 mg L<sup>-1</sup> each, Scheme S2). The pH of the resulting multidye solution was measured to be 7.4. Dye removal was monitored by UV–vis spectroscopy as a function of time (1–120 min), with concentrations quantitatively determined using calibration curves obtained from single-component aqueous solutions at the characteristic absorption maxima of each dye (Fig. S4). To ensure accurate quantification within the linear Beer–Lambert regime, aliquots (1 mL) withdrawn at selected time intervals were diluted to 3 mL prior to analysis, resulting in absorbance values below 1.0; measured concentrations were subsequently corrected for the dilution factor and used to calculate dye removal efficiencies relative to the initial concentration.

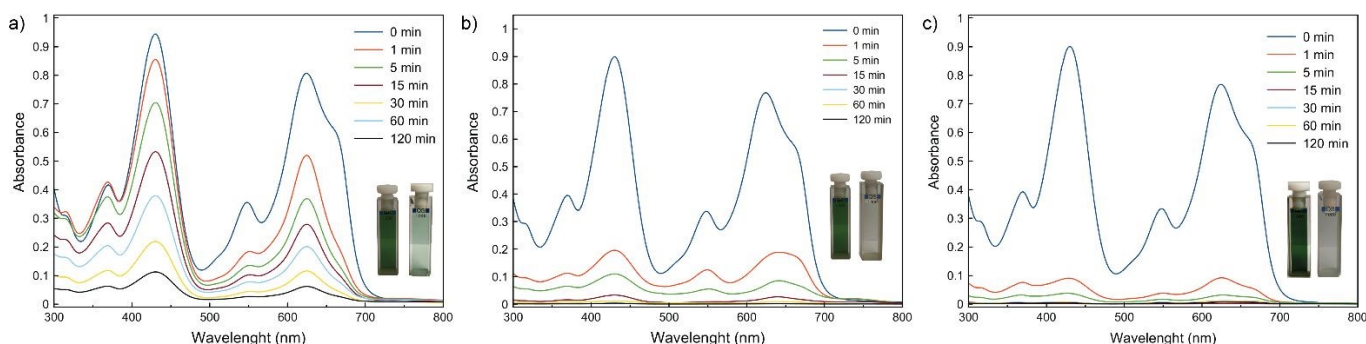


**Fig. 2.** Evolution with time of the UV-Vis absorption spectra of a multidye solution containing 10 ppm solutions of Auramine O, Brilliant green, Methylene blue and Pyronin Y in real water samples from Turia river in the presence of 50 mg of MOF 1 (a), MOF 2 (b), MTV-MOF 3 (c). The photographs show the colours of the solutions at the beginning (left) and after 30 minutes of exposure of the multidye solution with the corresponding (MTV)-MOF (right).

Under identical experimental conditions, MOF 1 showed only a moderate dye uptake (Figs. 2a and S5 and Table S1). In turn, MOF 2 –bearing larger and more flexible –CH<sub>2</sub>CH<sub>2</sub>SCH<sub>3</sub> side chains– exhibited significantly faster kinetics and higher removal efficiencies, being capable to remove virtually all four dyes in only 30 min (Figs. 2b and S6 and Table S1). This behaviour is in line with previous observations reported for the analogous Cu<sub>6</sub>Ca-based MOF.<sup>46</sup> Remarkably, the multivariate MOF 3 displayed an even better performance, achieving quantitative removal of all dyes within only 15 min (Figs. 2c and S7 and Table S1). Although the precise molecular origin of this behaviour cannot be unequivocally established from the

present data, the coexistence of distinct sulfur-functionalized environments within MTV-MOF 3 may contribute to the observed improvement in adsorption kinetics and dye removal efficiency, as observed previously.<sup>39</sup>

To further evaluate whether the improved performance of MTV-MOF 3 arises simply from the simultaneous presence of both monofunctional components, additional control experiments were performed using a physical 1:1 mixture of MOFs 1 and 2 under identical conditions (Figs. S8 and Table S2). The adsorption behaviour of the physical mixture was found to be approximately intermediate between those of the parent materials and significantly inferior to that of MTV-MOF 3. These



results indicate that the enhanced adsorption performance of MTV-MOF **3** cannot be reproduced by a simple physical combination of MOFs **1** and **2** and are consistent with a beneficial effect associated with the chemically heterogeneous environment generated within the multivariate framework.

### 2.3 Preparation of calcium alginate-based spheres containing MOFs 1-3

Having established the intrinsic adsorption performance of the powdered MOFs toward the multidye system, we next addressed their processing into macroscopic and mechanically robust forms suitable for practical deployment.<sup>27–29</sup> To improve material handling, facilitate recovery from aqueous media and enable potential integration into capture devices, MOFs **1–3** were incorporated into calcium alginate matrices to form spherical composite beads (Fig. 3).<sup>35</sup> The resulting hybrid calcium alginate spheres are hereafter referred to as **CAS-1**, **CAS-2** and **CAS-3**, respectively. Alginate-based shaping has been previously explored as a means to enhance the applicability of MOF adsorbents, with reported examples including in situ ZIF-8/alginate<sup>53</sup> (and other MOFs<sup>54–56</sup>) gels for pharmaceutical removal,<sup>53</sup> MOF–alginate beads for ion capture from seawater,<sup>57</sup> and UiO-66 or magnetic MOF composites for heavy metal and dye adsorption.<sup>58–61</sup> These studies highlight the promise of alginate as a sustainable processing platform for MOF-based adsorbents.

Nevertheless, many reported systems rely on MOFs with limited chemical tuneability, target single-component pollutants or exhibit partial loss of porosity and adsorption efficiency upon encapsulation within the polymer matrix.<sup>62</sup> Moreover, adsorption studies are most often conducted under dispersive batch conditions, while demonstrations under continuous-flow or solid-phase extraction (SPE) operation<sup>50–52</sup>—more relevant for realistic and time-efficient water treatment—remain scarce. In particular, systematic evidence showing that shaping strategies can fully preserve the intrinsic performance of highly crystalline and functionally complex MOFs, including under multicontaminant adsorption conditions, repeated use and flow-through operation, is still limited. In this context, alginate spheres provide an ideal platform to assess whether advanced MOF designs, including multivariate frameworks, can be translated into processable, robust and reusable adsorbents without compromising adsorption efficiency or structural integrity.

In this context, we focused our efforts on the preparation of alginate-based hybrid spheres incorporating the highest possible loading of MOFs **1–3**, while preserving the adsorption properties observed for the corresponding polycrystalline powders (see Experimental Section and Fig. 3). A sodium alginate (SA) aqueous solution was prepared by dissolving 0.25 g of SA in 15 mL of deionized water under stirring at 60 °C for 1 h in a thermostated water bath. Subsequently, 0.25 g of MOFs **1**, **2** and **3**, respectively, were added to the alginate solutions, in separate experiments, under continuous stirring, affording homogeneous white gelatinous suspensions. To eliminate entrapped air bubbles and ensure uniform dispersion of the MOF particles, the suspensions were subjected to ultrasonic water-bath treatment for 30 min. The resulting mixtures were then added dropwise, using a 25 mL syringe, into a 4 wt% aqueous CaCl<sub>2</sub> solution, leading to instantaneous crosslinking and the formation of spherical hydrogel beads. Finally, the obtained alginate spheres were thoroughly washed with deionized water for 24 h and stored in water (Fig. S9) prior to further characterization and adsorption studies.

The morphology, composition and structural integrity of the alginate-based hybrid spheres **CAS-1**, **CAS-2** and **CAS-3** were thoroughly characterized by a combination of powder X-ray diffraction (PXRD), nitrogen adsorption measurements, scanning electron microscopy (SEM), energy-dispersive X-ray spectroscopy (SEM–EDX) and elemental (CHNS) analyses. PXRD patterns recorded for the freshly prepared spheres match well with those of the corresponding powdered MOFs (Fig. S10), confirming that the crystalline frameworks are preserved during the alginate encapsulation process. Importantly, PXRD measurements performed on the spheres after storage in water for three months reveal no detectable structural degradation, highlighting the excellent hydrolytic stability of the composites under prolonged aqueous conditions (Fig. S11).

Nitrogen adsorption isotherms measured at 77 K show that the alginate spheres retain permanent porosity, with maximum N<sub>2</sub> uptake values corresponding to approximately 50% of those observed for the powdered materials (Fig. S12). This result is fully consistent with the MOF loading in the spheres, which was determined to be ca. 50 wt% by both CHNS and SEM–EDX analyses (Figs. S13–S15)—which show a very homogeneous distribution of MOFs' particles within the spheres—and indicates that the accessible

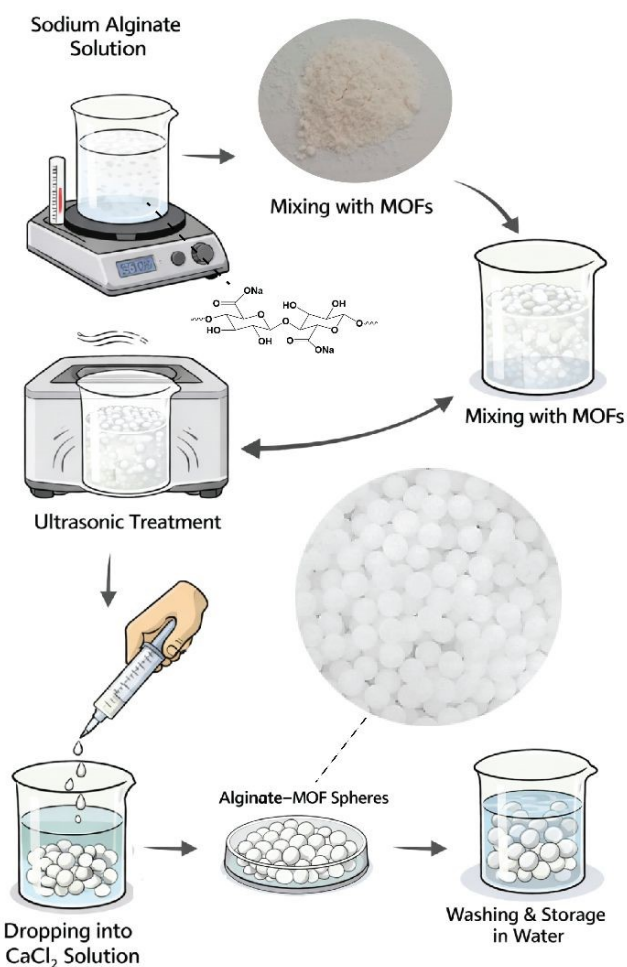


Fig. 3. Synthetic route for the preparation of calcium alginate-based spheres containing MOFs **1–3** (named **CAS-1**, **CAS-2** and **CAS-3**, respectively).



porosity of the MOFs is largely preserved upon shaping. SEM images further reveal the formation of uniform spherical beads with well-defined morphology, in which the MOF microcrystals are homogeneously embedded within the alginate matrix and remain clearly discernible (Figs. 4 and S16-S17). Collectively, these results

demonstrate that alginate-based processing enables high MOF loadings while preserving crystallinity, porosity and long-term stability, thereby providing robust and processable adsorbents suitable for water remediation applications.

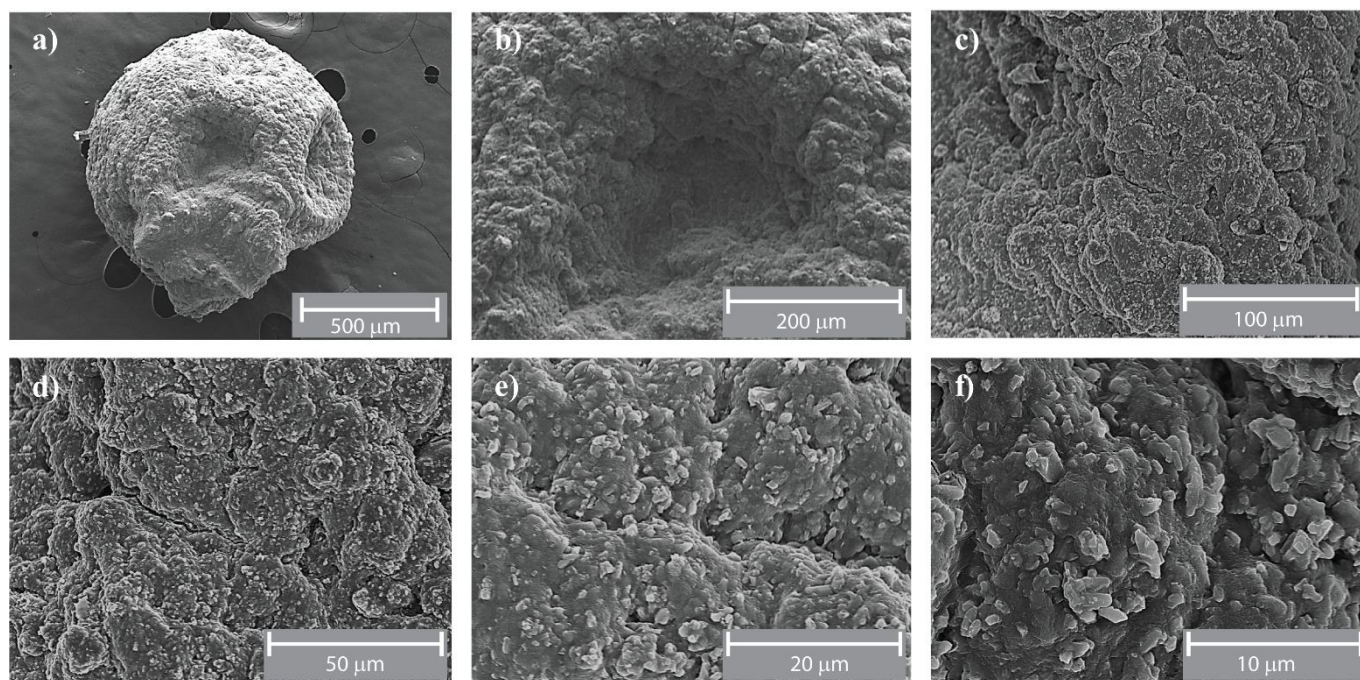


Fig. 4. (a) SEM image of a single calcium alginate sphere of CAS-1 (a) and (b-f) different zoomed areas of the sphere.

#### 2. 4 Capture experiments of calcium alginate spheres

The adsorption performance of the alginate-based spheres containing MOFs (CAS-1, CAS-2 and CAS-3) was next evaluated under batch conditions using the same multidye aqueous solution (AO, PY, BG and MB; 10 mg L<sup>-1</sup> each) employed for the powdered materials. In these experiments, 50 mg of spheres were contacted –under continuous stirring– with 25 mL of the multidye solution, and the dye removal was monitored by UV–vis spectroscopy as a function of time. Notably, the alginate spheres exhibit adsorption profiles and overall removal efficiencies that closely reproduce (Figs. 5 and S18-S34 and Tables S3-S5) those observed for the corresponding powdered MOFs 1-3 (Figs. 2 and S5-S7), achieving quantitative dye removal within comparable timescales. A slightly slower uptake kinetics is observed for the spheres, which can be rationalized by their effective MOF content (*ca.* 50 wt%, corresponding to ~25 mg of MOF per experiment), compared to the 50 mg of pure MOF used in the powder-based studies.

To evaluate the contribution of the alginate matrix itself, control experiments were performed using pristine calcium alginate spheres prepared under identical conditions but in the absence of MOFs. These control spheres exhibited only negligible dye uptake under the investigated conditions (Fig. S35 and Table S6), confirming that the adsorption performance of CAS-1, CAS-2 and CAS-3 is predominantly governed by the embedded MOF particles, while the alginate matrix mainly acts as a mechanically robust shaping and supporting medium.

Importantly, the alginate spheres display excellent reusability. Each material was subjected to five consecutive adsorption cycles, showing essentially unchanged capture efficiencies relative to the first cycle (Figs. 5 and S18-S34 and Tables S3-S5). Regeneration between cycles was achieved by simply suspending the spheres in a water/methanol (1:1 v/v) mixture for 30 s, followed by direct reuse without any additional treatment. To further evaluate the efficiency of the regeneration procedure, the washing solutions obtained after treatment of dye-loaded CAS materials with a water/methanol (1:1 v/v) mixture were analysed by UV–vis spectroscopy. Desorption efficiencies in the 45–60% range were observed for the different dyes after a contact time shorter than 30 s (Table S7), demonstrating the rapid release of a significant fraction of the adsorbed guests during the regeneration step. The preservation of adsorption performance over multiple cycles highlights the robustness of the alginate–MOF composites and demonstrates that shaping into spherical beads does not compromise the intrinsic adsorption properties of the parent MOFs. Moreover, the structural integrity of the best performing material embedded in alginate spheres (CAS-3), after the five consecutive capture cycles, was established by measuring PXRD patterns after the fifth cycle (Fig. S36).

The total adsorption capacities under the experimental conditions ( $q_e$ ) employed in this work were approximately 18 mg g<sup>-1</sup> for CAS-1 and 20 mg g<sup>-1</sup> for both CAS-2 and CAS-3 when referred to the total mass of the composite material.



Considering the ca. 50 wt% MOF loading of the spheres, these values correspond to approximately 36 mg g<sup>-1</sup> (**CAS-1**) and 40 mg g<sup>-1</sup> (**CAS-2** and **CAS-3**) when normalized to the actual MOF content. These values represent adsorption capacities under

the experimental conditions employed and should not be interpreted as maximum adsorption capacities ( $Q_{max}$ ) derived from adsorption isotherms.

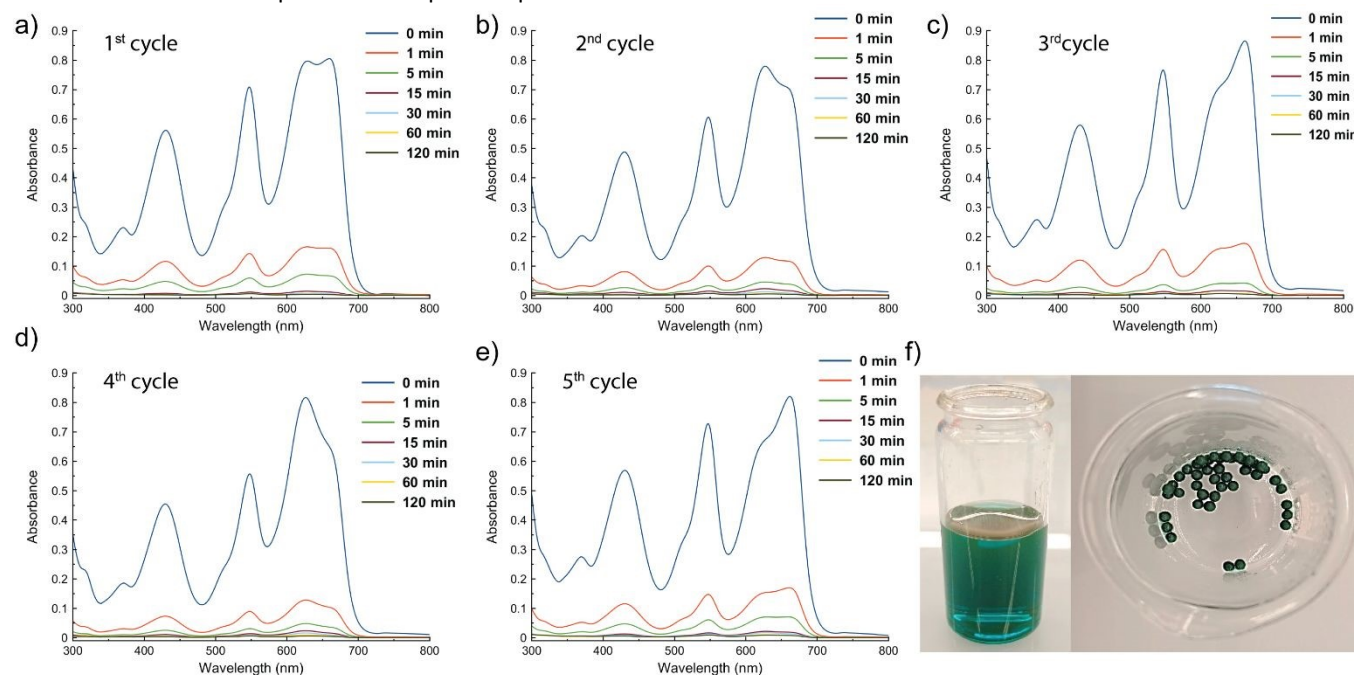


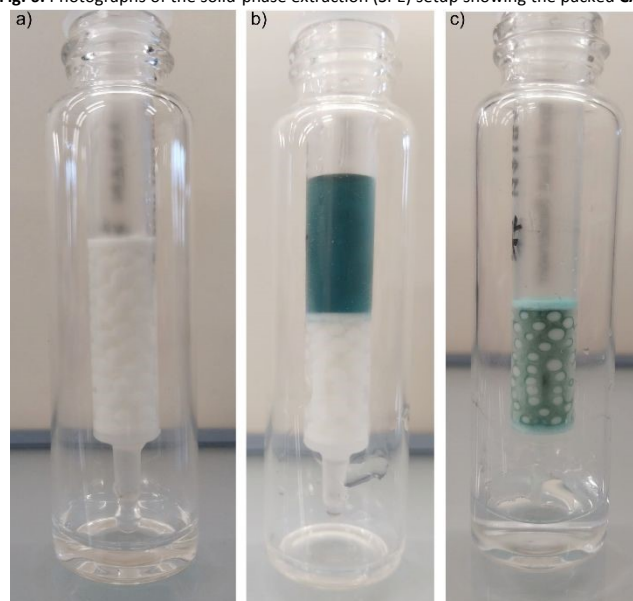
**Fig. 5.** Time evolution of the UV-Vis absorption spectra of a multidye solution containing 10 mg L<sup>-1</sup> each of Auramine O, Brilliant Green, Methylene Blue, and Pyronin Y in real water samples from the Turia River, in the presence of 50 mg of **CAS-3**, over five consecutive cycles (a–e). (f) Photograph of the multidye solution before the capture experiments (left) and image of **CAS-3** spheres together with the resulting colourless solution after 120 minutes in the fifth capture cycle (right).

Since **CAS-1**, **CAS-2** and **CAS-3** are hydrogel-based composites, they are intended to be stored and used in the hydrated state, whereas drying leads to irreversible shrinkage and hardening of the beads. Under hydrated conditions, the CAS materials retained their spherical morphology without visible swelling, deformation or disintegration after storage in water for more than three months (Fig. S37). This observation, together with the preservation of crystallinity after repeated adsorption/desorption cycles (Fig. S36), further demonstrates the excellent operational stability of the alginate–MOF composites.

To evaluate the influence of pH on the performance and stability of the best-performing material (**CAS-3**), additional adsorption experiments were conducted at pH 4 and pH 10. In both cases, the material retained high dye removal efficiencies (Fig. S38 and Table S8) and preserved its crystallinity after the adsorption experiments, as confirmed by PXRD analysis (Fig. S39). These results indicate that **CAS-3** remains structurally stable and functional under moderately acidic and basic conditions.

Finally, the practical applicability of the alginate-based spheres was evaluated under continuous-flow conditions using a solid-phase extraction (SPE) setup (Fig. 6), where 25 mg of the best performing spheres (**CAS-3**) were packed into a 10 mL polypropylene column (Fig. 6a) and confined between two porous frits (0.5 cm pore size).

**Fig. 6.** Photographs of the solid-phase extraction (SPE) setup showing the packed **CAS-3**



(a), the multidye aqueous solution prior to percolation (b), and the colorless solution collected after passing through the column (c).

The resulting SPE device was then challenged with a 5 mL multidye aqueous solution (MB, BG, PY, and AO; 10 mg L<sup>-1</sup> each) under gravity-flow conditions (Fig. 6b). The percolated solution exited the column colourless and was subsequently analysed by UV–vis spectroscopy. Remarkably, dye removal efficiencies exceeding 99% were obtained for all four dyes (Fig. S40 and



Table S9), demonstrating quantitative decontamination under flow-through conditions.

Compared to batch adsorption experiments, the SPE configuration enables significantly faster processing while maintaining—and even slightly improving—removal efficiencies. This enhanced performance can be attributed to the establishment of multiple dynamic adsorption equilibria along the packed bed, which promote efficient contact between the solution and the active MOF sites. The effectiveness of this process is visually illustrated in Fig. S6, which shows the packed CA spheres (Fig. S6a), the deep green contaminated solution prior to entering the column (Fig. S6b), and the completely colourless solution exiting the column (Fig. S6c). Overall, these results highlight the suitability of alginate-shaped multivariate

MOFs for continuous and time-efficient water remediation, further underscoring the advantages of combining advanced MOF design with sustainable shaping strategies.

In order to place the performance of the present system into context, a comparison with representative MOF–alginate composites previously reported for pollutant removal is provided in Table 1. Although direct quantitative comparisons are inherently complicated by differences in pollutant identity, concentration, adsorbent loading and operating conditions, the comparison reveals that the present CAS materials combine several features that are rarely reported simultaneously, including rapid multidyedye removal, operation in real river water, excellent recyclability and successful implementation under continuous-flow SPE conditions.

**Table 1.** Representative MOF–alginate composites reported for pollutant removal and comparison with the present work.

Material	MOF	Pollutant system	Water matrix	Reusability	Flow operation	Key observation	Ref.
ZIF-8/alginate beads	ZIF-8	Pharmaceutical pollutant	DI water	Yes	No	In situ gel formation; pollutant removal	53
MOF/alginate beads	Various MOFs	Single-component pollutants	DI water	Yes	No	General proof-of-concept for MOF immobilization	54–56
MOF–alginate beads	MOF composite	Metal ions from seawater	Seawater	Yes	No	Ion capture from complex matrix	57
UiO-66/alginate beads	UiO-66	Heavy metals / dyes	DI water	Yes	No	Retained adsorption after shaping	58
Magnetic MOF/alginate composites	Magnetic MOF	Dyes	DI water	Yes	No	Easy magnetic recovery	59–61
<b>CAS-3</b> (This work)	MTV-MOF	Multidyedye system (AO, PY, BG, MB)	Real river water (Turia)	5 cycles	Yes (SPE)	Quantitative removal, fast kinetics, flow-through operation	This work

### 3. Conclusions

This work demonstrates how the combination of rational MOF design and sustainable shaping strategies can enhance the practical applicability of MOF-based adsorbents for real-world water remediation. Two monofunctional sulfur-functionalized MOFs (**1** and **2**) and a multivariate analogue (**3**) were investigated toward the removal of a multidyedye aqueous system. The MTV-MOF **3** displays slightly faster adsorption kinetics and superior capture performance, underscoring the potential benefits of chemically heterogeneous pore environments for multicomponent pollutant removal.

Although the precise origin of this performance enhancement cannot be unequivocally established, it is likely associated with the coexistence of linkers of different length and flexibility within the framework. The elongated methionine-based ligand present in MOF **2** may contribute enhanced conformational adaptability, potentially facilitating kinetically favoured sequestration of contaminants. In parallel, the shorter methylcysteine-derived linker (MOF **1**), which preserves similar chemical functionality, may provide increased accessible volume, enabling dye molecules to adopt more favourable orientations within the channels. The combination of these features in the MTV-MOF may therefore promote cooperative

host–guest interactions arising from both flexible anchoring sites and accessible pore space. Such a heterogeneous environment is expected to favour the stabilization of guest species through a network of non-covalent interactions, including van der Waals contacts and  $\sigma$ -hole interactions, consistent with the rapid and quantitative removal observed experimentally.

Importantly, all MOFs were successfully processed into calcium alginate spheres with high MOF loadings (*ca.* 50%), while fully retaining crystallinity, permanent porosity and hydrolytic stability. The alginate-shaped materials reproduce the adsorption performance of the powdered MOFs, showing fast and quantitative dye removal under batch conditions, excellent reusability over multiple cycles and preserved structural integrity. Furthermore, solid-phase extraction experiments confirm quantitative dye removal under continuous-flow operation, enabling faster and more efficient decontamination compared to dispersive adsorption.

Overall, this study highlights alginate-based shaping as a simple, sustainable and effective route to translate advanced and functionally complex MOFs into robust, reusable and flow-compatible adsorbents, bridging the gap between molecularly designed MOFs and realistic water remediation technologies.



## Conflicts of interest

There are not conflicts of interest to declare.

## Data availability

The data supporting this article have been included as part of the ESI<sup>†</sup>. Any other data would be available upon reasonable request from the authors.

## Acknowledgements

This work was supported by MCIN (projects CNS2024-154962, PID2022-136349OB-I00 and Excellence Unit "Maria de Maeztu" (CEX2024-001467-M)), and by the Ministero dell'Istruzione, dell'Università e della Ricerca (Italy). D.A. gratefully acknowledge financial support from the Italian Ministero dell'Università e della Ricerca (MUR) under the PRIN 2022 call (Prot. 20224HH9KP, project MUR: 20224HH9KP\_002). Thanks are also extended to the "Generalitat Valenciana" (Project PROMETEO/2021/054) and the "Ramón y Cajal Program", RYC2019-027940-I (J. F.-S.). This study forms part of the Advanced Materials programme (MFA/2022/048) and was supported by MCIN with funding from European Union NextGenerationEU (PRTR-C17.11) and by Generalitat Valenciana. E.P. acknowledges the financial support of the European Research Council under the European Union's Horizon 2020 research and innovation programme / ERC Grant Agreement No 814804, MOF-reactors.

## Notes and references

- 1 A. Tkaczyk, K. Mitrowska and A. Posyniak, *Sci. Total Environ.*, 2020, **717**, 137222.
- 2 L. Dsikowitzky and J. Schwarzbauer, *Environ. Chem. Lett.*, 2014, **12**, 371–386.
- 3 T. Akter, A. T. Protity, M. Shaha, M. Al Mamun and A. Hashem, *The Impact of Textile Dyes on the Environment*, Springer Nature Singapore, 2023, pp. 401–431.
- 4 H. Kolya and C.-W. Kang, *Toxics*, 2024, **12**, 111.
- 5 G. Bal and A. Thakur, *Mater. Today Proc.*, 2022, **50**, 1575–1579.
- 6 A. Ahmad, S. H. Mohd-Setapar, C. S. Chuong, A. Khatoon, W. A. Wani, R. Kumar and M. Rafatullah, *RSC Adv.*, 2015, **5**, 30801–30818.
- 7 F. J. Alguacil and F. A. López, *Molecules*, 2021, **26**, 5440.
- 8 R. Rashid, I. Shafiq, P. Akhter, M. J. Iqbal and M. Hussain, *Environ. Sci. Pollut. Res.*, 2021, **28**, 9050–9066.
- 9 K. E. Ukhurebor, I. Hossain, K. Pal, G. Jokthan, F. Osang, F. Ebrima and D. Katal, *Top. Catal.*, 2024, **67**, 140–155.
- 10 I. Ali and V. K. Gupta, *Nat. Protoc.*, 2006, **1**, 2661–2667.
- 11 S. Satyam and S. Patra, *Heliyon*, 2024, **10**, e29573.
- 12 H. Furukawa, K. E. Cordova, M. O'Keeffe and O. M. Yaghi, *Science*, 2013, **341**, 974.
- 13 H.-C. Zhou and S. Kitagawa, *Chem. Soc. Rev.*, 2014, **43**, 5415–5418.
- 14 Y. Cui, B. Li, H. He, W. Zhou, B. Chen and G. Qian, *Acc. Chem. Res.*, 2016, **49**, 483–493.
- 15 O. K. Farha and J. T. Hupp, *Acc. Chem. Res.*, 2010, **43**, 1166–1175.
- 16 M. Mon, R. Bruno, J. Ferrando-Soria, D. Armentano and E. Pardo, *J. Mater. Chem. A*, 2018, **6**, 4912–4947.
- 17 C. Negro, W. D. Guerra, D. Armentano, J. Ferrando-Soria, T. Grancha and E. Pardo, *Chem. Commun.*, 2024, **60**, 14935–14951.
- 18 Y. Wen, P. Zhang, V. K. Sharma, X. Ma and H.-C. Zhou, *Cell Reports Phys. Sci.*, 2021, **2**, 100348.
- 19 S. Rojas and P. Horcajada, *Chem. Rev.*, 2020, **120**, 8378–8415.
- 20 G. Wu, J. Ma, S. Li, J. Li, X. Wang, Z. Zhang and L. Chen, *J. Mater. Chem. A*, 2023, **11**, 6747–6771.
- 21 R. M. Rego, G. Kuriya, M. D. Kurkuri and M. Kigga, *J. Hazard. Mater.*, 2021, **403**, 123605.
- 22 D. Jiang, M. Chen, H. Wang, G. Zeng, D. Huang, M. Cheng, Y. Liu, W. Xue and Z. Wang, *Coord. Chem. Rev.*, 2019, **380**, 471–483.
- 23 G. Sriram, A. Bendre, E. Mariappan, T. Altalhi, M. Kigga, Y. C. Ching, H.-Y. Jung, B. Bhaduri and M. Kurkuri, *Sustain. Mater. Technol.*, 2022, **31**, e00378.
- 24 E. M. Dias and C. Petit, *J. Mater. Chem. A*, 2015, **3**, 22484–22506.
- 25 Y. Yao, C. Wang, J. Na, M. S. A. Hossain, X. Yan, H. Zhang, M. A. Amin, J. Qi, Y. Yamauchi and J. Li, *Small*, 2022, **18**, 2104387.
- 26 U. Ryu, S. Jee, P. C. Rao, J. Shin, C. Ko, M. Yoon, K. S. Park and K. M. Choi, *Coord. Chem. Rev.*, 2021, **426**, 213544.
- 27 Y. Chen, X. Huang, S. Zhang, S. Li, S. Cao, X. Pei, J. Zhou, X. Feng and B. Wang, *J. Am. Chem. Soc.*, 2016, **138**, 10810–10813.
- 28 Z. Wang, L. Liu, Z. Li, N. Goyal, T. Du, J. He and G. K. Li, *Energy & Fuels*, 2022, **36**, 2927–2944.
- 29 Q. Ma, T. Zhang and B. Wang, *Matter*, 2022, **5**, 1070–1091.
- 30 A. Knebel, A. Bavykina, S. J. Datta, L. Sundermann, L. Garzon-Tovar, Y. Lebedev, S. Durini, R. Ahmad, S. M. Kozlov, G. Shterk, M. Karunakaran, I. D. Carja, D. Simic, I. Weilert, M. Klüppel, U. Giese, L. Cavallo, M. Rueping, M. Eddaoudi, J. Caro and J. Gascon, *Nat. Mater.*, 2020, **19**, 1346–1353.
- 31 Q. Hu, L. Xu, K. Fu, F. Zhu, T. Yang, T. Yang, J. Luo, M. Wu and D. Yu, *Nano Res.*, 2022, **15**, 2961–2970.
- 32 J. Zheng, X. Cui, Q. Yang, Q. Ren, Y. Yang and H. Xing, *Chem. Eng. J.*, 2018, **354**, 1075–1082.
- 33 H. Yang and J. R. Wright, in *Cell Encapsulation Technology and Therapeutics*, Birkhäuser Boston, Boston, MA, 1999, pp. 79–89.
- 34 F. Kurul, B. Doruk and S. N. Topkaya, *Discov. Chem.*, 2025, **2**, 68.
- 35 B. -B. Lee, P. Ravindra and E. -S. Chan, *Chem. Eng. Technol.*, 2013, **36**, 1627–1642.
- 36 B. Wang, Y. Wan, Y. Zheng, X. Lee, T. Liu, Z. Yu, J. Huang, Y. S. Ok, J. Chen and B. Gao, *Crit. Rev. Environ. Sci. Technol.*, 2019, **49**, 318–356.
- 37 A. Helal, Z. H. Yamani, K. E. Cordova and O. M. Yaghi, *Natl. Sci. Rev.*, 2017, **4**, 296–298.
- 38 M. Viciano-Chumillas, X. Liu, A. Leyva-Pérez, D. Armentano, J. Ferrando-Soria and E. Pardo, *Coord. Chem. Rev.*, 2022, **451**, 214273.
- 39 M. Mon, R. Bruno, E. Tiburcio, M. Viciano-Chumillas, L. H. G. Kalinke, J. Ferrando-Soria, D. Armentano and E. Pardo, *J. Am. Chem. Soc.*, 2019, **141**, 13601–13609.
- 40 M. Baratta, T. F. Mastropietro, P. Escamilla, V. Algieri, F. Xu, F. P. Nicoletta, J. Ferrando-Soria, E. Pardo, G. De Filipo and D. Armentano, *Inorg. Chem.*, 2024, **63**, 18992–19001.
- 41 P. Escamilla, N. Moliner, D. Armentano, E. Pardo, J. Ferrando-Soria and T. Grancha, *Magnetochemistry*, 2024, **10**, 99.
- 42 P. Escamilla, M. Monteleone, R. M. Percoco, T. F. Mastropietro, M. Longo, E. Esposito, A. Fuoco, J. C. Jansen, R. Elliani, A. Tagarelli, J. Ferrando-Soria, V. Amendola, E. Pardo and D. Armentano, *ACS Appl. Mater. Interfaces*, 2024, **16**, 51182–51194.
- 43 C. Bilanin, P. Escamilla, J. Ferrando-Soria, A. Leyva-Pérez, D. Armentano and E. Pardo, *Dalton Trans.*, 2023, **52**, 18018–18026.



- 44 C. Negro, H. Martínez Pérez-Cejuela, E. F. Simó-Alfonso, J. M. Herrero-Martínez, R. Bruno, D. Armentano, J. Ferrando-Soria and E. Pardo, *ACS Appl. Mater. Interfaces*, 2021, **13**, 28424–28432.
- 45 M. Mon, R. Bruno, E. Tiburcio, P.-E. Casteran, J. Ferrando-Soria, D. Armentano and E. Pardo, *Chem. Eur. J.*, 2018, **24**, 17712–17718.
- 46 C. Negro, P. Escamilla, R. Bruno, J. Ferrando-Soria, D. Armentano and E. Pardo, *Chem. Eur. J.*, 2022, **28**, e202200034.
- 47 P. Escamilla, L. Bartella, S. Sanz-Navarro, R. M. Percoco, L. Di Donna, M. Prejanò, T. Marino, J. Ferrando-Soria, D. Armentano, A. Leyva-Pérez and E. Pardo, *Chem. Eur. J.*, 2023, **29**, e202301325.
- 48 S. Brunauer, P. H. Emmett and E. Teller, *J. Am. Chem. Soc.*, 1938, **60**, 309–319.
- 49 C. Negro, H. Martínez Pérez-Cejuela, E. F. Simó-Alfonso, W. Iqbal, J. M. Herrero-Martínez, D. Armentano, J. Ferrando-Soria and E. Pardo, *ACS Appl. Mater. Interfaces*, 2023, **15**, 3069–3076.
- 50 L. García, P. García-Atienza, S. Armenta, J. M. Herrero-Martínez, M. Prejanò, T. Marino, D. Armentano, T. Grancha, J. Ferrando-Soria and E. Pardo, *J. Mater. Chem. A*, 2025, **13**, 42204–42214.
- 51 T. Grancha, P. García-Atienza, L. García, S. Armenta, J. M. Herrero-Martínez, D. Armentano, T. F. Mastropietro, J. Ferrando Soria and E. Pardo, *Small*, 2025, **21**, e10000.
- 52 T. Grancha, P. Garcia-Atienza, S. Armenta, J. M. Herrero-Martínez, R. M. Percoco, D. Armentano, J. Ferrando-Soria and E. Pardo, *J. Mater. Chem. A*, 2025, **13**, 24473–24482.
- 53 R. Yu and Z. Wu, *Environ. Technol.*, 2023, **44**, 2395–2406.
- 54 F. Zhang, D. Zhang, X. Ran, M. Xiao, L. Gan, X. Yang, Y. Xie and Q. Sun, *Colloids Surfaces B Biointerfaces*, 2025, **256**, 115082.
- 55 M. G. El-Desouky, A. A. Alayyafi, G. A. A. M. Al-Hazmi and A. A. El-Bindary, *J. Mol. Liq.*, 2024, **399**, 124392.
- 56 B. Chen, Y. Li, Q. Du, X. Pi, Y. Wang, Y. Sun, M. Wang, Y. Zhang, K. Chen and J. Zhu, *Nanomaterials*, 2022, **12**, 2897.
- 57 S. J. Lee, T. Hann and S. H. Park, *ACS Appl. Mater. Interfaces*, 2020, **12**, 16319–16326.
- 58 S. Daradmare, M. Xia, V. N. Le, J. Kim and B. J. Park, *Chemosphere*, 2021, **270**, 129487.
- 59 T. Wu, J. Lei, L. Lin, Q. Wang, T. H. Farooq, G. Wang, J. Wang and W. Yan, *Environ. Technol. Innov.*, 2023, **32**, 103428.
- 60 L. Cheng, Y. Lu, P. Li, B. Sun and L. Wu, *Molecules*, 2025, **30**, 1560.
- 61 Z. Ye, H. Zhang, G. Zhou, Z. Bai, J. Jiang, R. Yang, Y. Wang and F. Quan, *Int. J. Biol. Macromol.*, 2024, **281**, 136286.
- 62 S. K. Gebremariam, A. M. Varghese, S. Ehrling, Y. Al Wahedi, A. AlHajaj, L. F. Dumée and G. N. Karanikolos, *ACS Appl. Mater. Interfaces*, 2024, **16**, 50785–50799.

View Article Online  
DOI: 10.1039/D6DT01043A





Valencia, May 5th, 2026

### **Data availability statement**

The data supporting this article have been included as part of the ESI†. Any other data would be available upon reasonable request from the authors.

Yours sincerely,

Dr Emilio Pardo

